



# Cytoplasmic synthesis of endogenous *Alu* complementary DNA via reverse transcription and implications in age-related macular degeneration

Shinichi Fukuda<sup>a,b,c,1</sup>, Akhil Varshney<sup>a,b,1</sup>, Benjamin J. Fowler<sup>d</sup>, Shao-bin Wang<sup>a,b</sup>, Siddharth Narendran<sup>a,b,e</sup>, Kameshwari Ambati<sup>a,b</sup>, Tetsuhiro Yasuma<sup>d,f</sup>, Joseph Magagnoli<sup>g,h</sup>, Hannah Leung<sup>a,b</sup>, Shuichiro Hirahara<sup>a,b,i</sup>, Yosuke Nagasaka<sup>a,b</sup>, Reo Yasuma<sup>a,b,f</sup>, Ivana Apicella<sup>a,b</sup>, Felipe Pereira<sup>a,b,j</sup>, Ryan D. Makin<sup>a,b</sup>, Eamonn Magner<sup>k</sup>, Xinan Liu<sup>k</sup>, Jian Sun<sup>a,b</sup>, Mo Wang<sup>l</sup>, Kirstie Baker<sup>l</sup>, Kenneth M. Marion<sup>l</sup>, Xiwen Huang<sup>k</sup>, Elmira Baghdasaryan<sup>l,m</sup>, Meenakshi Ambati<sup>a,b,n</sup>, Vidya L. Ambati<sup>n</sup>, Akshat Pandey<sup>a,b</sup>, Lekha Pandya<sup>a,b</sup>, Tammy Cummings<sup>g,h</sup>, Daipayan Banerjee<sup>a,b</sup>, Peirong Huang<sup>a,b</sup>, Praveen Yerramothu<sup>a,b</sup>, Genrich V. Tolstonog<sup>o</sup>, Ulrike Held<sup>p</sup>, Jennifer A. Erwin<sup>q</sup>, Apua C. M. Paquola<sup>q</sup>, Joseph R. Herdy<sup>r</sup>, Yuichiro Ogura<sup>l</sup>, Hiroko Terasaki<sup>f</sup>, Tetsuro Oshika<sup>c</sup>, Shaban Darwish<sup>s,t</sup>, Ramendra K. Singh<sup>s</sup>, Saghar Mozaffari<sup>s</sup>, Deepak Bhattarai<sup>u</sup>, Kyung Bo Kim<sup>u</sup>, James W. Hardin<sup>g,v</sup>, Charles L. Bennett<sup>g,h,w</sup>, David R. Hinton<sup>x,y</sup>, Timothy E. Hanson<sup>z,aa</sup>, Christian Röver<sup>bb</sup>, Keykavous Parang<sup>s</sup>, Nagaraj Kerur<sup>a,b,cc,dd</sup>, Jinze Liu<sup>k</sup>, Brian C. Werner<sup>ee</sup>, S. Scott Sutton<sup>g,h</sup>, Srinivas R. Sadda<sup>l,m</sup>, Gerald G. Schumann<sup>p</sup>, Bradley D. Gelfand<sup>a,b,ff</sup>, Fred H. Gage<sup>r,2</sup>, and Jayakrishna Ambati<sup>a,b,dd,gg,2</sup>

<sup>a</sup>Center for Advanced Vision Science, School of Medicine, University of Virginia, Charlottesville, VA 22908; <sup>b</sup>Department of Ophthalmology, School of Medicine, University of Virginia, Charlottesville, VA 22908; <sup>c</sup>Department of Ophthalmology, University of Tsukuba, Ibaraki 305-8575, Japan; <sup>d</sup>Department of Ophthalmology and Visual Sciences, University of Kentucky, Lexington, KY 40536; <sup>e</sup>Aravind Eye Hospital System, Madurai 625020, India; <sup>f</sup>Department of Ophthalmology, Graduate School of Medicine, Nagoya University, Nagoya 464-8601, Japan; <sup>g</sup>Dorn Research Institute, Columbia Veterans Affairs Health Care System, Columbia, SC 29208; <sup>h</sup>Department of Clinical Pharmacy and Outcomes Sciences, College of Pharmacy, University of South Carolina, Columbia, SC 29208; <sup>i</sup>Department of Ophthalmology, Graduate School of Medical Sciences, Nagoya City University, Nagoya 467-8601, Japan; <sup>j</sup>Departamento de Oftalmologia e Ciências Visuais, Escola Paulista de Medicina, Universidade Federal de São Paulo, São Paulo 04023-062, Brazil; <sup>k</sup>Department of Computer Science, University of Kentucky, Lexington, KY 40536; <sup>l</sup>Doheny Eye Institute, Los Angeles, CA 90033; <sup>m</sup>Department of Ophthalmology, David Geffen School of Medicine, University of California, Los Angeles, CA 90095; <sup>n</sup>Center for Digital Image Evaluation, Charlottesville, VA 22901; <sup>o</sup>Department of Otolaryngology–Head and Neck Surgery, University Hospital of Lausanne, 1011 Lausanne, Switzerland; <sup>p</sup>Department of Medical Biotechnology, Paul Ehrlich Institute, 63225 Langen, Germany; <sup>q</sup>The Lieber Institute for Brain Development, School of Medicine, Johns Hopkins University, Baltimore, MD 21205; <sup>r</sup>Laboratory of Genetics, Salk Institute for Biological Studies, La Jolla, CA 92037; <sup>s</sup>Center for Targeted Drug Delivery, Department of Biomedical and Pharmaceutical Sciences, School of Pharmacy, Chapman University, Irvine, CA 92618; <sup>t</sup>Organometallic and Organometalloid Chemistry Department, National Research Centre, Giza 12622, Egypt; <sup>u</sup>Department of Pharmaceutical Sciences, University of Kentucky, Lexington, KY 40536; <sup>v</sup>Department of Epidemiology and Biostatistics, University of South Carolina, Columbia, SC 29208; <sup>w</sup>Center for Medication Safety and Efficacy, College of Pharmacy, University of South Carolina, Columbia, SC 29208; <sup>x</sup>Department of Ophthalmology, University of Southern California Roski Eye Institute, Keck School of Medicine, University of Southern California, Los Angeles, CA 90033; <sup>y</sup>Department of Pathology, Keck School of Medicine, University of Southern California, Los Angeles, CA 90033; <sup>z</sup>Medtronic, Inc., Minneapolis, MN 55432; <sup>aa</sup>Division of Biostatistics, School of Public Health, University of Minnesota, Minneapolis, MN 55455; <sup>bb</sup>Department of Medical Statistics, University Medical Center Göttingen, D-37073 Göttingen, Germany; <sup>cc</sup>Department of Neuroscience, School of Medicine, University of Virginia, Charlottesville, VA 22908; <sup>dd</sup>Department of Pathology, School of Medicine, University of Virginia, Charlottesville, VA 22908; <sup>ee</sup>Department of Orthopaedic Surgery, School of Medicine, University of Virginia, Charlottesville, VA 22908; <sup>ff</sup>Department of Biomedical Engineering, School of Medicine, University of Virginia, Charlottesville, VA 22908; and <sup>gg</sup>Department of Microbiology, Immunology, and Cancer Biology, School of Medicine, University of Virginia, Charlottesville, VA 22908

Contributed by Fred H. Gage, December 28, 2020 (sent for review November 4, 2020; reviewed by Maria B. Grant, Carl Schmid, and Kang Zhang)

***Alu* retroelements propagate via retrotransposition by hijacking long interspersed nuclear element-1 (L1) reverse transcriptase (RT) and endonuclease activities. Reverse transcription of *Alu* RNA into complementary DNA (cDNA) is presumed to occur exclusively in the nucleus at the genomic integration site. Whether *Alu* cDNA is synthesized independently of genomic integration is unknown. *Alu* RNA promotes retinal pigmented epithelium (RPE) death in geographic atrophy, an untreatable type of age-related macular degeneration. We report that *Alu* RNA-induced RPE degeneration is mediated via cytoplasmic L1–reverse-transcribed *Alu* cDNA independently of retrotransposition. *Alu* RNA did not induce cDNA production or RPE degeneration in L1-inhibited animals or human cells. *Alu* reverse transcription can be initiated in the cytoplasm via self-priming of *Alu* RNA. In four health insurance databases, use of nucleoside RT inhibitors was associated with reduced risk of developing atrophic macular degeneration (pooled adjusted hazard ratio, 0.616; 95% confidence interval, 0.493–0.770), thus identifying inhibitors of this *Alu* replication cycle shunt as potential therapies for a major cause of blindness.**

*Alu* | retrotransposon | macular degeneration | retina | health insurance databases

Reverse transcription of RNA into DNA occurs as part of the replication cycle of retroelements, genetic elements that reproduce via a copy-and-paste mechanism using a retrotransposon-encoded

Author contributions: J.A. designed research; S.F., A.V., B.J.F., S.-b.W., S.N., K.A., T.Y., J.M., H.L., S.H., Y.N., R.Y., I.A., R.D.M., E.M., X.L., J.S., M.W., K.B., K.M.M., X.H., E.B., M.A., V.L.A., A.P., L.P., T.C., D. Banerjee, P.H., P.Y., U.H., J.A.E., A.C.M.P., J.R.H., D. Bhattarai, K.B.K., J.W.H., C.L.B., T.E.H., C.R., K.P., N.K., J.L., B.C.W., S.S.S., S.R.S., G.G.S., B.D.G., and J.A. performed research; G.V.T., Y.O., H.T., T.O., S.D., R.K.S., S.M., D.R.H., and G.G.S. contributed new reagents/analytic tools; S.F., A.V., B.J.F., S.-b.W., S.N., K.A., T.Y., J.M., H.L., S.H., Y.N., I.A., R.D.M., E.M., X.L., J.S., M.W., K.B., K.M.M., X.H., E.B., M.A., V.L.A., A.P., L.P., T.C., D. Banerjee, P.H., P.Y., U.H., J.A.E., A.C.M.P., J.R.H., D. Bhattarai, K.B.K., J.W.H., C.L.B., T.E.H., C.R., K.P., N.K., J.L., B.C.W., S.S.S., S.R.S., G.G.S., B.D.G., F.H.G., and J.A. analyzed data; and S.F., A.V., B.J.F., S.N., R.Y., F.P., N.K., G.G.S., B.D.G., and J.A. wrote the paper.

Reviewers: M.B.G., University of Alabama at Birmingham; C.S., University of California, Davis; and K.Z., Macau University of Science and Technology.

Competing interest statement: J.A. is a co-founder of iVeena Holdings, iVeena Delivery Systems, and Inflammasome Therapeutics, and has been a consultant for Allergan, Biogen, Boehringer-Ingelheim, Immunovant, Janssen, Olix Pharmaceuticals, Retinal Solutions, and Saksin LifeSciences unrelated to this work. J.A., B.D.G., B.J.F., S.N., K.A., S.-b.W., I.A., M.A., F.P., N.K., and S.F. are named as inventors on patent applications on macular degeneration filed by the University of Virginia or the University of Kentucky. J.W.H. has received consulting fees from Celgene Corporation unrelated to this work. S.S.S. has received research grants from Boehringer Ingelheim, Gilead Sciences, Portola Pharmaceuticals, and United Therapeutics unrelated to this work. J.A. and B.D.G. are co-founders of DiceRx.

Published under the [PNAS license](#).

<sup>1</sup>S.F. and A.V. contributed equally to this work.

<sup>2</sup>To whom correspondence may be addressed. Email: [gage@salk.edu](mailto:gage@salk.edu) or [ja9qr@virginia.edu](mailto:ja9qr@virginia.edu).

This article contains supporting information online at <https://www.pnas.org/lookup/suppl/doi:10.1073/pnas.2022751118/-DCSupplemental>.

Published February 1, 2021.

## Significance

*Alu* elements, comprising more than 10% of the human genome, propagate via retrotransposition. This genomic expansion requires enzymatic activity of L1 that reverse transcribes *Alu* RNA into *Alu* cDNA in the nucleus. We report *Alu* also undergoes L1-mediated reverse transcription via self-priming in the cytoplasm independent of retrotransposition, providing evidence of human DNA synthesis in this cellular compartment. This newly discovered shunt molecule in the *Alu* replication cycle also induces death of the retinal pigmented epithelium, a hallmark of atrophic age-related macular degeneration. A Big Data Archeology analysis of multiple health insurance databases reveals that use of FDA-approved nucleoside reverse transcriptase inhibitors is associated with protection against macular degeneration, identifying a repurposing candidate for this blinding disease.

reverse transcriptase (RT). Retroelements have multiplied to occupy ~42% of the human genome (1), yet the fate of retroelement-derived cDNA not integrated into the genome is poorly understood.

Age-related macular degeneration (AMD) is a blinding disease that affects 180 million people (2). In geographic atrophy, an advanced vision-threatening form of AMD without effective therapies (3), *Alu* RNA expressed from endogenous *Alu* retrotransposons by RNA polymerase III accumulates in the retinal pigmented epithelium (RPE) (4, 5). *Alu* RNA induces RPE cytotoxicity in human cells and mice; surprisingly, numerous RNA sensors are dispensable for this toxicity, and several other structurally similar RNAs are not toxic to the RPE (4, 6, 7). Therefore, we explored the replication cycle of the nonautonomous retrotransposon *Alu*, which includes reverse transcription of the *Alu* RNA by the L1-encoded RT *in trans* at the nuclear genomic insertion site—termed target-primed reverse transcription (TPRT)—and integration of the *Alu* cDNA into the genome (8–10).

Here, we demonstrate the existence of endogenous reverse-transcribed *Alu* cDNA synthesized in the cytoplasm of human cells independently of TPRT and provide evidence that *Alu* RNA can undergo self-priming to form *Alu* cDNA in the cytoplasm. We also present evidence from four independent patient health records databases that nucleoside reverse transcriptase inhibitor (NRTI) use is associated with reduced development of atrophic AMD; thus, these clinically approved drugs potentially could be repurposed for this disease.

## Results

**L1 Is Required for *Alu* RNA Toxicity.** Previously, we demonstrated NRTIs have two distinct inhibitory targets: RT and the NLRP3 inflammasome (11). While the RT-inhibitory function was dispensable for the anti-inflammatory effects of NRTIs, whether reverse transcription of *Alu* RNA is required for its toxicity was not tested. Thus, we examined whether endogenous L1-encoded RT mediated *Alu* RNA toxicity because L1-encoded ORF2p harboring RT and endonuclease (EN) activities can use *Alu* RNA as a template for reverse transcription *in trans* (12, 13).

We identified two mouse L1 (mL1) small interfering RNAs (siRNAs) that reduced endogenous L1 ORF2p abundance in mouse RPE cells (*SI Appendix, Fig. S1 A and B*). Subretinal delivery of either mL1 siRNA, synthesized in a cell-permeable, nonimmunogenic format (14, 15), prevented *Alu* RNA-induced RPE degeneration in wild-type (WT) mice (Fig. 1*A* and *SI Appendix, Figs. S1C and S2A*). These similar outcomes argue against off-target siRNA activity; nevertheless, several mRNAs contain embedded sequences corresponding to varying L1 segments. However, mouse mRNAs containing sequences complementary to

mL1 siRNA were not down-regulated following mL1 siRNA treatment in mouse RPE cells (*SI Appendix, Fig. S1D*). Next, we performed *in vivo* functional rescue of endogenous L1 RT via either of two expression plasmids: one encoding a synthetic and codon-optimized full-length human L1 element [pORFeus-Hs (16)] and the other encoding rat L1 ORF2p [pORF2-Rn (17)] (*SI Appendix, Fig. S1E*). Both these siRNA-refractory L1 expression constructs restored *Alu* RNA toxicity in mice despite coadministering mL1 siRNAs (*SI Appendix, Fig. S1 F and G*). These data suggest L1 activity is necessary and sufficient for *Alu* RNA toxicity in mice.

Next, we studied whether retrotransposition, i.e., genomic insertion of reverse-transcribed *Alu* cDNA, which occurs infrequently in somatic cells, was responsible for *Alu* RNA toxicity. We synthesized a mutant *Alu* element with two mutations (G25C/G159C) (Fig. 1*B*), which has diminished retrotransposition ability (18). Despite retrotransposition deficiency, reconfirmed in a transmobilization assay (Fig. 1*C*), *Alu* G25C/G159C RNA induced RPE degeneration in WT mice (Fig. 1*D* and *SI Appendix, Fig. S2B*) in a dose-dependent manner alike WT *Alu* RNA (*SI Appendix, Fig. S3 A and B*). *Alu* G25C/G159C toxicity was prevented by the NRTI lamivudine (3TC) (Fig. 1*E* and *SI Appendix, Fig. S2C*) or mL1 siRNA (Fig. 1*F* and *SI Appendix, Fig. S2D*). Olaparib, a chemical inhibitor of L1 retrotransposition (19), inhibited *Alu* retrotransposition (*SI Appendix, Fig. S4A*) but did not block reverse transcription of *Alu* RNA into *Alu* cDNA in primary human RPE cells (*SI Appendix, Fig. S4B*) or *Alu* RNA-induced RPE degeneration in WT mice (Fig. 1*G* and *SI Appendix, Fig. S2E*). These findings suggest L1-mediated reverse transcription, but not retrotransposition, is essential for *Alu* RNA toxicity. Hence, we hypothesized that *Alu* cDNA reverse transcribed by L1 RT but not inserted into the genome is a key intermediate in *Alu* RNA toxicity.

**Reverse-Transcribed *Alu* cDNA in Cells and Mice.** We generated a strand-specific probe to detect endogenous single-stranded *Alu* cDNA (*SI Appendix, Fig. S5 A–C*). Using *in situ* hybridization, we detected an artificially synthesized single-stranded *Alu* DNA transfected into primary human RPE cells in a dose-dependent manner; this signal was abolished by single-strand-specific S1 nuclease (*SI Appendix, Fig. S5B*). We next developed a variation of nucleic acid blotting that we term “equator blotting”: a functional combination of northern and Southern blotting (*SI Appendix, Supplementary Methods*) to detect extrachromosomal DNAs and their size. An equator blot is similar to a Southern blot in that it probes for a target DNA sequence, yet unlike a typical Southern blot, does not involve restriction enzyme digestion of the DNA. Instead, the DNA is separated without enzyme digestion prior to hybridization, per the typical northern blot procedure. Hence, we refer to the procedure of hybridization of undigested DNA as an equator blot. *Alu* RNA and *Alu* cDNA were probed in nuclear and cytoplasmic fractions. A probe recognizing U6 RNA was hybridized to fractions before RNase A treatment to confirm successful nuclear fractionation. Equator blotting using the *Alu*-specific probe, we detected accumulation of *Alu* cDNA, ~300 nt in length, after *Alu* RNA transfection in primary human RPE cells; this signal was resistant to RNase A and double-stranded DNase but sensitive to S1 nuclease (*SI Appendix, Fig. S5C*), consistent with its specificity for nongenomic *Alu* sequences.

Using equator blotting and *in situ* hybridization, we assessed whether *Alu* cDNA synthesis is modulated by titrating *Alu* RNA levels. Increasing *Alu* RNA levels by any of three methods [transfection of *in vitro* transcribed synthetic RNA (4), heat shock (20), or *DICER1* knockdown by antisense oligonucleotide (4)] induced *Alu* cDNA formation, which was abrogated by inhibition of endogenous RT with 3TC in primary human RPE cells (Fig. 2*A* and *B* and *SI Appendix, Figs. S6 and S7 A–D*). This

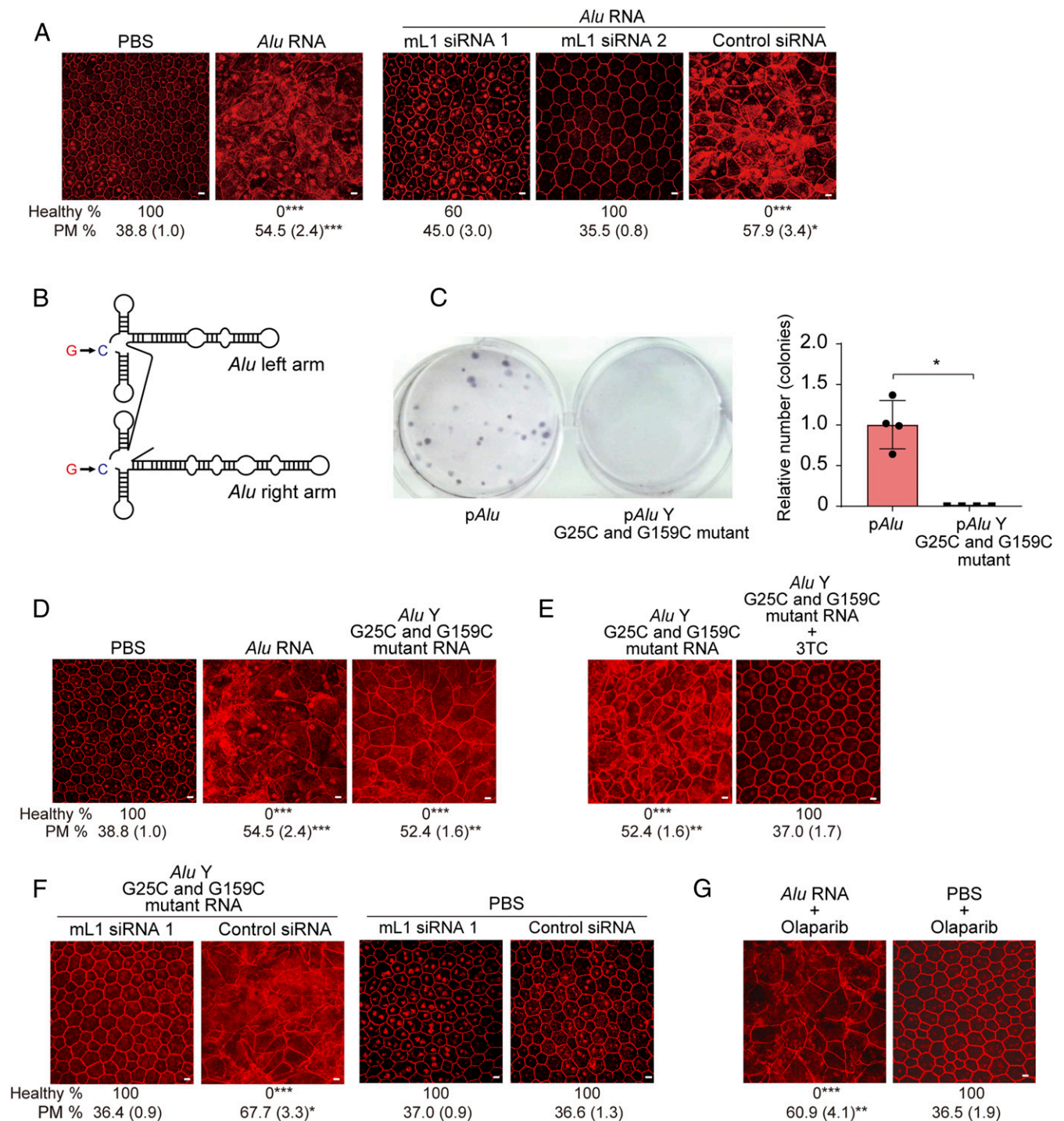


**Fig. 1.** Endogenous L1 is required for *Alu* RNA-induced RPE toxicity. (A) RPE sheet micrographs of mice. RPE cellular boundaries were visualized by immunostaining flat mounts with zonula occludens-1 (ZO-1, red) antibody. Loss of regular hexagonal cellular boundaries in flat mounts represents degenerated RPE. (Scale bars, 10  $\mu$ m.) Binary and morphometric quantification of RPE degeneration are shown. (\* $P < 0.05$ ; \*\* $P < 0.01$ ; \*\*\* $P < 0.001$ , Fisher's exact test for binary; two-tailed  $t$  test for morphometry.) PM, polymegethism [mean (SEM)]. RPE morphology in wild-type (WT) mice administered with *Alu* RNA or PBS, and *Alu* RNA with either of two L1-targeted siRNAs or control siRNA.  $n = 6-15$ . (B) Schematic of secondary structure of an *Alu* RNA harboring G25C/G159C mutations. (C) Retrotransposition frequency of *Alu* G25C/G159C double mutant RNA compared to *Alu* RNA in a cellular *Alu* retrotransposition reporter assay (described in *SI Appendix, Supplementary Methods*). \* $P < 0.05$ , Mann-Whitney  $U$  test. The error bars represent the mean  $\pm$  SEM. (D and E) RPE morphology in WT mice following administration of *Alu* RNA or *Alu* G25C/G159C double-mutant RNA. (Scale bars, 10  $\mu$ m.)  $n = 6$ . (E) *Alu* G25C/G159C double-mutant RNA-induced RPE degeneration in WT mice was blocked by 3TC. (Scale bars, 10  $\mu$ m.)  $n = 5-6$ . (F) *Alu* G25C/G159C double-mutant RNA or PBS subretinal injection into WT mice with mL1 siRNA or control siRNA. (Scale bars, 10  $\mu$ m.)  $n = 6-11$ . (G) RPE degeneration (ZO-1 flat mounts) in WT mice treated with *Alu* RNA and olaparib, a chemical inhibitor of L1 retrotransposition. (Scale bars, 10  $\mu$ m.)  $n = 4-7$ .

endogenous *Alu* cDNA was ~300 nt long (Fig. 2A), suggesting it does not correspond to *Alu* sequences in fragmented genomic DNA. Little or no *Alu* cDNA was observed in untreated cells, suggesting it was newly synthesized and that the detection methodology was not identifying genomic DNA.

*Alu* cDNA accumulation resulting from all three methods was predominantly cytoplasmic (Fig. 2B and *SI Appendix*, Fig. S6); however, following *DICER1* knockdown, *Alu* cDNA was occasionally nuclear (*SI Appendix*, Fig. S7C). S1 nuclease eliminated the *Alu* cDNA signal, confirming it as single-stranded DNA (*SI Appendix*, Fig. S7D). These data confirm RT activity is required for generating *Alu* cDNA.

To quantify reverse transcription of *Alu* RNA into *Alu* cDNA, we subjected cytoplasmic fractions of primary human RPE cells to adaptor-based PCR quantification (*Alu* c-PCR) (*SI Appendix*, Fig. S8 A–F). This method avoids detecting circular forms of extrachromosomal *Alu* DNAs (*SI Appendix*, Fig. S8B) (21). 3TC down-regulated *Alu* cDNA in primary human RPE cells (*SI Appendix*, Fig. S8A), suggesting reverse transcription of endogenous *Alu* RNA generates *Alu* cDNA in human RPE cells. Increased levels of *Alu* cDNA in primary human RPE cells following transfection of in vitro transcribed *Alu* RNA, heat shock, or

*DICER1* knockdown were abolished by 3TC in primary human RPE cells (Fig. 2C), further confirming endogenous RT activity is required for generating *Alu* cDNA under conditions that elevate *Alu* RNA levels.

Using in situ hybridization of RPE whole mounts, we tested whether *Alu* cDNA was generated in mice after subretinal *Alu* RNA transfection. We performed this study using mice functionally deficient in the inflammasome components caspase-1 and caspase-4 (termed Casp1/4 dko mice), which are protected from *Alu* RNA toxicity (6, 22), to visualize *Alu* cDNA signals free of distortions arising from degenerating cells. In these mice, *Alu* cDNA accumulation was detected after *Alu* RNA transfection and blocked by 3TC, suggesting *Alu* cDNA production in vivo required reverse transcription (*SI Appendix*, Fig. S9).

***Alu* cDNA Formation Requires Human L1 RT Activity.** Two human L1 (hL1) siRNAs that down-regulated endogenous L1 ORF2 in primary human RPE cells (*SI Appendix*, Fig. S10 A and B) prevented *Alu* cDNA production in primary human RPE cells after *Alu* RNA transfection, heat shock, or *DICER1* antisense treatment, as monitored by in situ hybridization (*SI Appendix*, Fig. S11) and real-time PCR (Fig. 2D). In situ hybridization revealed hL1

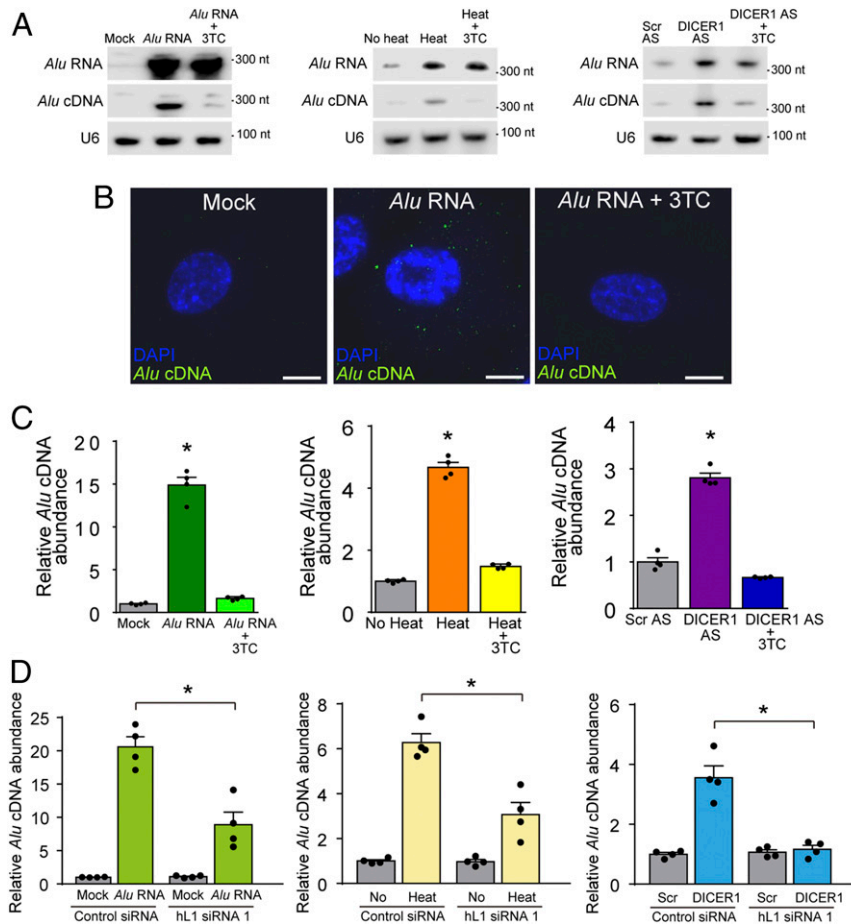


**Fig. 2.** Endogenous L1 reverse-transcribed cytoplasmic *Alu* cDNA. (A) Northern blotting for *Alu* RNA (top bands), equator blotting for *Alu* cDNA (middle bands), and northern blotting for U6 RNA (bottom bands) of cytoplasmic fractions of primary human RPE cells transfected with *Alu* RNA, exposed to heat shock, or transfected with a *DICER1*-targeted antisense oligonucleotide (*DICER1* AS) in the presence or absence of 3TC. Representative of  $n = 3$  experiments. (B) Fluorescent micrographs of in situ hybridization of *Alu* cDNA in human RPE cells (green) colabeled with DAPI (blue) to identify nuclei. Cells were transfected with *Alu* RNA in the presence or absence of 3TC. Representative of  $n = 3$  experiments. (Scale bar, 10  $\mu\text{m}$ .) (C) *Alu* c-PCR of cytoplasmic fractions of primary human RPE cells transfected with *Alu* RNA, exposed to heat shock, or transfected with a *DICER1* AS in the presence or absence of 3TC. Representative of  $n = 3$  experiments. \* $P < 0.05$ , Mann–Whitney  $U$  test. (D) Direct amplification by real-time PCR (without reverse transcription) of *Alu* cDNA in primary human RPE cells treated with in vitro-transcribed *Alu* RNA, heat shock, or *DICER1* AS after transfection with hL1 siRNA #1 compared with control siRNA. \* $P < 0.05$  by Mann–Whitney  $U$  test.  $n = 4$ . Error bars show SEM.

siRNA down-regulated *Alu* cDNA in ARPE-19 cells after heat shock and *DICER1* antisense treatments (*SI Appendix, Fig. S12*). Conversely, L1 overexpression enhanced *Alu* cDNA production in *Alu* RNA-transfected ARPE-19 cells (*SI Appendix, Fig. S13*).

Supportive of the idea that reverse transcription, but not retrotransposition, is essential for *Alu* RNA toxicity, the retrotransposition-deficient *Alu* G25C/G159C RNA (Fig. 1 *B* and *C*), which induced RPE degeneration in WT mice (Fig. 1*D* and *SI Appendix, Fig. S2B*), also induced *Alu* cDNA formation in mouse embryonic carcinoma F9 cells and primary human RPE cells (*SI Appendix, Fig. S14 A and B*) and in vivo in Casp1/4 dko mice (*SI Appendix, Fig. S14C*). These data demonstrate *Alu* cDNA is produced and exerts toxicity in the absence of L1-mediated *Alu* retrotransposition.

We investigated *Alu* cDNA formation in multiple human cell types using direct amplification by real-time PCR. Basal levels of endogenous *Alu* cDNA varied more than 100-fold among 11 different primary cells and cell lines (*SI Appendix, Fig. S15*). Among the cells tested, those with the highest expression of endogenous *Alu* cDNA were, in order of abundance, NTera2D cells, primary human peripheral mononuclear cells, ARPE-19 cells, primary human RPE cells, and human embryonic kidney 293-T cells.

Since *Alu* exhibit sequence heterogeneity, we investigated from which *Alu* subfamilies the identified *Alu* cDNA sequences were derived. *Alu* sequences are broadly grouped into J, S, and Y families based on sequence divergence throughout millions of years of genomic *Alu* element propagation (23–25). We performed next-generation sequencing of cytoplasmic fractions of primary human RPE cells, restricted to 200- to 800-nt-long species to exclude genomic DNA contamination and embedded *Alus*. *AluS* and *AluJ* sequences were overrepresented in the cytoplasmic fractions covering ~92% of all obtained reads, whereas *AluY* reads comprised ~8% (*SI Appendix, Fig. S16A*). These fractions are comparable to the distribution of subfamilies of expressed Pol III-derived *Alu* RNAs in multiple cell types (26–28) (*SI Appendix, Fig. S16B*).

**Cytoplasmic Synthesis of *Alu* cDNA.** Canonically, reverse transcription of *Alu* RNA by L1 is thought to occur in the nucleus, coupled with genomic integration of *Alu* DNA. However, whether *Alu* cDNA is also synthesized in the cytoplasm is unknown. To determine the locus of synthesis of *Alu* cDNA that is not genomically integrated via TPRT, we used 3TC formulations that restrict it to either nuclear or cytoplasmic compartments. Conjugation of a cyclic peptide (Cpep) targets 3TC for nuclear localization (29), whereas a mixture of an amino acid/fatty acyl moiety (PA-4) restricts 3TC to the cytoplasm (30). Consistent with the model that TPRT of *Alu* RNA occurs in the nucleus and results in *Alu* retrotransposition, we confirmed that Cpep-3TC, but not PA-4-3TC, blocked *Alu* retrotransposition (Fig. 3 *A* and *B*). Conversely, cytoplasmic *Alu* cDNA formation in primary human RPE cells and *Alu* RNA-induced RPE degeneration in WT mice were blocked by PA-4-3TC but not Cpep-3TC (*SI Appendix, Fig. S17 A and B*), indicating that inhibition of cytoplasmic RT activity is critical for preventing *Alu* RNA toxicity and that toxic *Alu* cDNA did not leak from nucleus to cytoplasm following aborted *Alu* retrotransposition.

We then performed an ex vivo reverse transcription assay of *Alu* cDNA synthesis by incubating *Alu* RNA with protein extracts of nuclear or cytoplasmic fractions of WT mouse RPE cells or F9 cells, which have robust L1 expression (31). We observed higher amounts of synthesized *Alu* cDNA with cytoplasmic fractions than with nuclear fractions in both cells (Fig. 3*C*). Heat denaturation of cytoplasmic fractions eliminated *Alu* cDNA synthesis (Fig. 3*D*), compatible with its formation by a heat-labile enzyme. Cytoplasmic fractions isolated from mL1 siRNA-treated cells

produced less *Alu* cDNA than from control siRNA-treated cells (Fig. 3*E*). Treatment of cytoplasmic extracts with AZT-triphosphate (AZT-TP), the active form of the NRTI zidovudine (AZT) that inhibits reverse transcription, reduced *Alu* cDNA synthesis, whereas diethyl-AZT (DE-AZT), an alkyl-modified NRTI derivative that does not block RT (11, 32), did not inhibit *Alu* cDNA formation (Fig. 3*F*). Furthermore, mouse platelets, which lack a nucleus and contain L1 ribonucleoprotein particles harboring endogenous L1 RT activity (33), also synthesize *Alu* cDNA following *Alu* RNA transfection (*SI Appendix, Fig. S18 A–C*). These data support the conclusion that *Alu* cDNA can be synthesized via L1-mediated reverse transcription in the cytoplasm and that this cytoplasmic *Alu* cDNA is responsible for its retinal cytotoxicity.

To monitor cytoplasmic *Alu* cDNA formation, we probed the association between L1 ORF2p, *Alu* RNA, and *Alu* cDNA in RNase H2-deficient biotinylated-*Alu* RNA-transfected HeLa cells expressing V5-tagged rat L1 ORF2p. Using pull-down assays, we captured the association of both *Alu* RNA and *Alu* cDNA with L1 ORF2p in cytoplasmic extracts (*SI Appendix, Fig. S19 A–C*). These data support a model in which *Alu* RNA associates with L1 ORF2p in the cytoplasm and is reverse transcribed into *Alu* cDNA.

Consistent with this concept, we detected RNA–DNA hybrids following *Alu* RNA transfection in mouse embryonic fibroblasts (MEFs) (*SI Appendix, Fig. S20*). Following biotin-labeled *Alu* RNA transfection and streptavidin-affinity pulldown, we detected *Alu* cDNA in the biotin-bound fraction, but a ~13-fold greater amount of *Alu* cDNA in the biotin-unbound fraction (*SI Appendix, Fig. S20A*), suggesting *Alu* RNA–*Alu* cDNA hybrids are transient, as the majority of *Alu* cDNA is not bound to *Alu* RNA. Evidence supportive of *Alu* RNA–*Alu* cDNA hybrid formation was also found by immunostaining using an antibody that recognizes RNA–DNA hybrids (34) (*SI Appendix, Fig. S20B*). Biotin-labeled *Alu* RNA stability was greater in *Rnaseh2*<sup>−/−</sup> MEFs compared to WT MEFs, suggesting RNaseH2 is involved in degrading *Alu* RNA in these hybrids (*SI Appendix, Fig. S20C*).

***Alu* cDNA Formation via Self-Priming.** We sought to determine how priming of *Alu* reverse transcription might occur in the cytoplasm given that the canonical model of *Alu* retrotransposition holds that reverse transcription of *Alu* RNA by L1-ORF2p occurs in the nucleus and via TPRT, wherein the endonuclease activity of L1 exposes an oligo-T stretch of genomic DNA that serves to prime reverse transcription of the 3′ oligo-A stretch of *Alu* RNA (35). *Alu* RNA is capable of intramolecular base pairing (36); therefore, we hypothesized *Alu* could be capable of self-priming using its 3′ polyU-stretch (Fig. 4*A*). Indeed, the repetitive rodent BC1 RNA can prime its own reverse transcription (37).

We disabled the potential self-priming capability of an in vitro-synthesized *Alu* RNA via 3′ capping with the chain terminators 2′,3′-dideoxythymidine-5′-triphosphate (ddTTP) or cordycepin (3′-deoxyadenosine) (Fig. 4*A*). Consistent with our hypothesis, transfection of uncapped *Alu* RNA into WT mouse RPE cells supported *Alu* cDNA formation, whereas transfection of 3′-capped *Alu* RNA species did not (Fig. 4*B*). Also supportive, incubating WT mouse RPE cell cytoplasmic protein extracts with uncapped *Alu* RNA in an in-tube RT assay performed in the absence of external DNA or RNA primers resulted in far more *Alu* cDNA synthesis than with 3′-capped *Alu* RNA (Fig. 4 *C* and *D*). As in vivo corroboration, subretinal administration of 3′-capped *Alu* RNA species did not induce RPE degeneration in WT mice (Fig. 4*E*).

Next, we tagged an *Alu* RNA by inserting an S1 aptamer sequence into its 3′ end (Fig. 4*F*) and transfected it into mouse F9 cells. We detected *Alu* cDNA formation in the cytoplasm of these cells and confirmed that the complementary S1 aptamer sequence was present in this *Alu* cDNA by using an *Alu*-specific

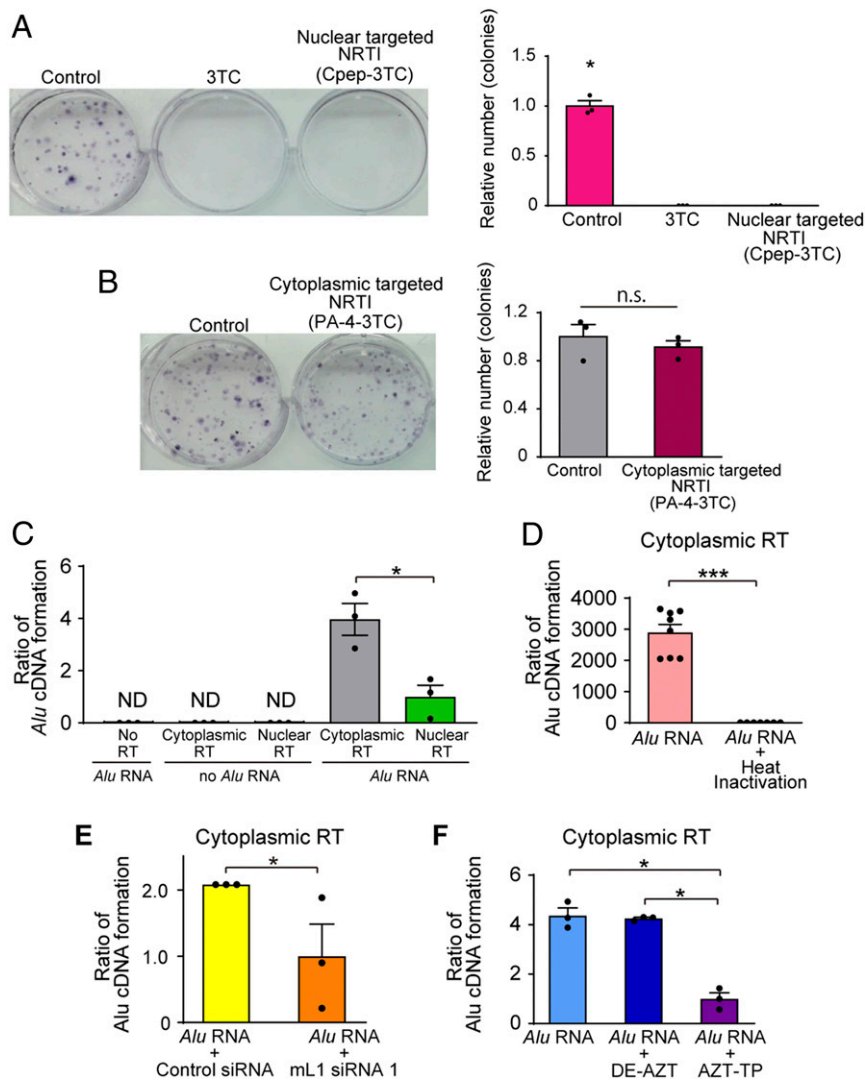


**Fig. 3.** *Alu* cDNA is synthesized in the cytoplasm. (A and B) *Alu* retrotransposition assays in the presence of (A) 3TC or nuclear targeted-3TC (Cpep-3TC), or (B) cytoplasmic-targeted 3TC (PA-4-3TC).  $n = 3$ . \* $P < 0.05$  by Mann–Whitney  $U$  test. Error bars show SEM. (C) Quantification of reverse transcription of *Alu* RNA by *Alu*-specific qPCR in cytoplasmic and nuclear fractions of mouse embryonal carcinoma F9 cells. (D) Quantification of *Alu* cDNA production in heat-inactivated cytoplasmic fractions.  $n = 7$ . (E) Quantification of *Alu* cDNA production in cytoplasmic fractions isolated from mouse L1 siRNA-treated cells. (F) Quantification of *Alu* cDNA production in cytoplasmic fractions of WT mouse RPE cells incubated with AZT-triphosphate (AZT-TP) or diethyl-AZT (DE-AZT).  $n = 3$ . \* $P < 0.05$ ; \*\*\* $P < 0.001$  by Mann–Whitney  $U$  test. Error bars show SEM.

forward primer and an S1 aptamer-specific reverse primer (Fig. 4F). These data demonstrate that *Alu* RNA can undergo self-priming to form *Alu* cDNA and suggest self-priming is one mechanism by which *Alu* reverse transcription is initiated in the cytoplasm.

**NRTIs Associated with Lower Risk of Atrophic Macular Degeneration in Humans.** We analyzed whether NRTI use was associated with altered risk of atrophic AMD in humans by analyzing four longitudinal health insurance databases in the United States: Truven MarketScan Commercial Claims; US Veterans Health Administration; PearlDiver Humana; and PearlDiver Mariner (SI Appendix, Tables S1–S5). In all four databases, fewer HIV-negative persons taking NRTIs for preexposure prophylaxis developed atrophic AMD compared to HIV-negative persons not taking NRTIs (SI Appendix, Table S1).

We analyzed the risk of developing atrophic AMD using Cox proportional hazards models, adjusting for age, gender, race,

body mass index, smoking, and Charlson Comorbidity Index score. NRTI exposure was associated with a reduced hazard of developing atrophic AMD (Fig. 5A) in Humana [adjusted hazard ratio (aHR) = 0.579; 95% confidence interval (CI), 0.439, 0.763] and Mariner (aHR = 0.676, 95% CI, 0.522, 0.876). Given the low event rate (38) among NRTI users in Truven and Veterans databases, we employed Bayesian proportional hazards Cox regression models: NRTI exposure was associated with a reduced hazard of atrophic AMD in Truven (aHR = 0.483; 95% CI, 0.430, 0.540) and Veterans (aHR = 0.776; 95% CI, 0.677, 0.917). Sensitivity analyses varying the weight allotted to the exponential distribution underlying the baseline hazard function in the Bayesian Cox models also revealed protective associations of NRTI use (SI Appendix, Table S6). We estimate the combined risk across databases based on an inverse-variance-weighted meta-analysis using random effects for two reasons. First, a large amount of the variance across studies is attributable to heterogeneity ( $I^2 = 83.1\%$ ; 95% CI, 49.3–98.6%;  $P < 0.001$ , test

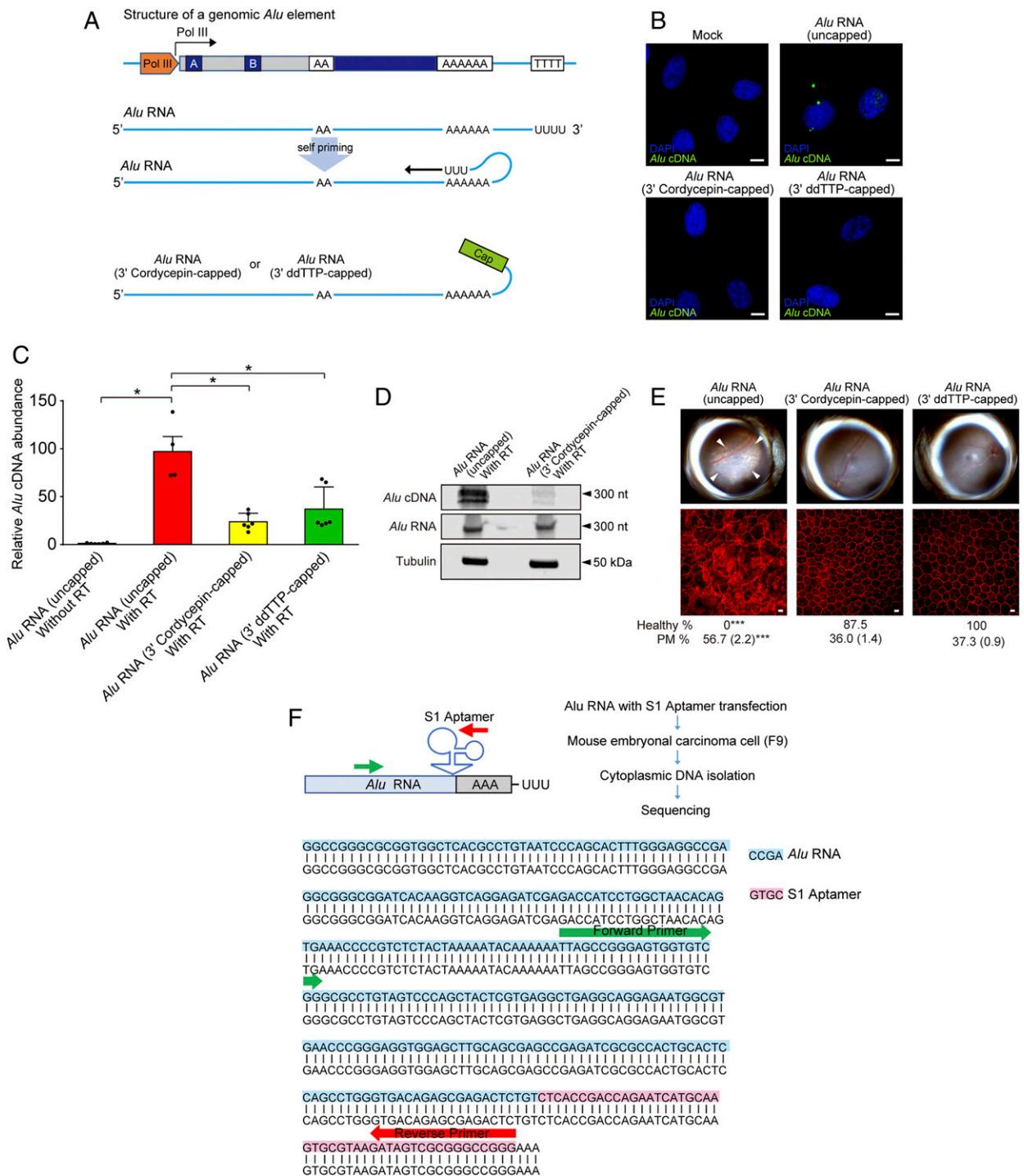


**Fig. 4.** *Alu* cDNA is synthesized via self-priming. (A) Schematic of putative *Alu* RNA transcription and self-priming by 3' complementary hybridization. *Alu* RNA was synthetically capped on the 3' end via dideoxy thymidine base (ddTTP) or cordycepin triphosphate to prevent extension via RT. (B) In situ hybridization of *Alu* cDNA after transfection of uncapped and or 3'-capped *Alu* RNAs into WT mouse RPE cells. Green, *Alu* cDNA; blue, DAPI. Representative of  $n = 3$  experiments. (Scale bar, 10  $\mu\text{m}$ .) (C) *Alu* cDNA abundance in cytoplasmic fractions of WT mouse RPE cells via an ex vivo RT activity assay (*S1* Appendix, Supplementary Methods), in the absence of external primers, followed by *Alu*-specific real-time PCR. PCR was performed with *Alu* RNA that was uncapped, or 3'-capped with ddTTP or cordycepin triphosphate.  $*P < 0.05$  by Mann-Whitney *U* test. (D) Blotting analysis of cytoplasmic fractions of WT mouse RPE cells to detect *Alu* cDNA, *Alu* RNA, and tubulin after performing an ex vivo RT activity assay in the absence of external primers (see above). Fractions were incubated with uncapped or 3'-cordycepin triphosphate-capped *Alu* RNA. (E) Fundus photographs (Top) and corresponding representative RPE sheet micrographs (Bottom) of WT mice administered uncapped *Alu* RNA or *Alu* RNAs capped on the 3' end with the chain ddTTP or cordycepin triphosphate. (Scale bars, 10  $\mu\text{m}$ .) The arrowheads in fundus image denote the boundaries of RPE hypopigmentation. Binary and morphometric quantification of RPE degeneration are shown.  $*P < 0.05$ ;  $**P < 0.01$ ;  $***P < 0.001$ , Fisher's exact test for binary; two-tailed *t* test for morphometry. PM, polymegethism [mean (SEM)].  $n = 6-8$ . (F) *Alu* RNA fused with S1 RNA aptamer at the 3' end (*Alu*-S1) was transfected into mouse embryonic carcinoma cells (mF9) cells. *Alu* cDNA was detected in the RNase-treated cytoplasmic fraction of these cells, and sequencing using an *Alu* specific-forward and S1 aptamer-specific reverse primer confirmed the presence of the complementary S1 aptamer sequence in this *Alu* cDNA.

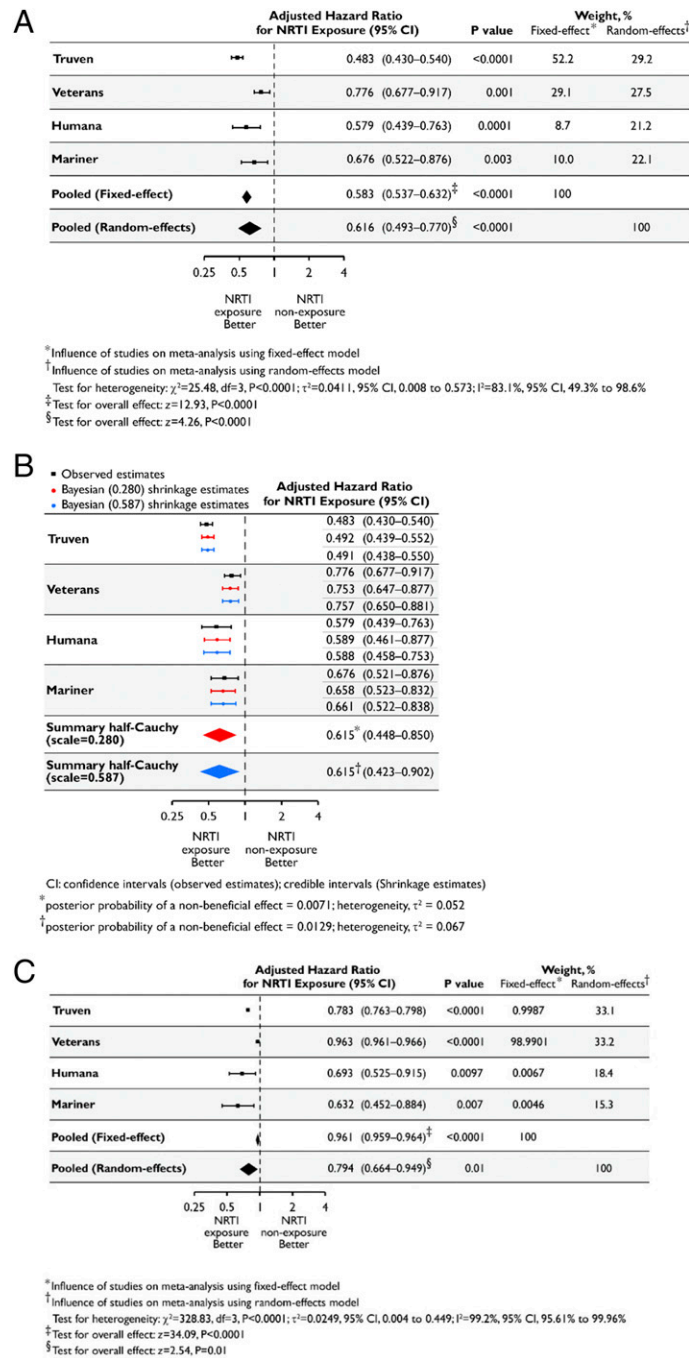


**Fig. 5.** NRTI use is associated with reduced hazard of incident atrophic AMD. (A–C) Using methodology employed in ref. 58, aHRs estimated separately for each database shown in black along with their 95% CIs, along with fixed-effect and random-effects meta-analyses shown in diamonds. The dashed vertical line denotes a HR of 1.0, which represents no difference in risk between nucleoside reverse-transcriptase inhibitor (NRTI) exposure and nonexposure. The horizontal bars represent 95% CIs. P values derived from z statistics for individual databases are reported. The estimates of heterogeneity ( $\tau^2$ ), results of the statistical test of heterogeneity using the  $\chi^2$  test statistic and its degrees of freedom (df), and posterior probabilities of a nonbeneficial effect for each model are shown below the plot. The Higgins  $I^2$  statistic and its 95% CI are presented. The results of the statistical tests of overall effect, the z-test statistics, and corresponding P values are presented. (A) HRs based on a Cox proportional-hazards model and adjusted for the confounding variables listed in *SI Appendix* were estimated separately for each database. Inverse-variance-weighted random-effects and fixed-effect meta-analyses were performed to obtain a pooled estimate of the aHR of incident atrophic AMD for NRTI exposure (ever vs. never). (B) HRs based on a Cox proportional-hazards model and adjusted for the confounding variables listed in *SI Appendix, Supplementary Methods*, were estimated separately for each database and are shown in black along with their 95% CIs. A Bayesian meta-analysis was performed using a random-effects model and a weakly informative hierarchical half-Cauchy prior distribution for between-study variance with the assumption that it was unlikely for the between-study HRs to vary by more than threefold (scale = 0.280). A sensitivity analysis to the choice of the prior by assuming that it was unlikely for the between-study HRs to vary by more than 10-fold was also performed (scale = 0.587). The Bayesian shrinkage estimates and the summary estimates of the aHR of incident atrophic AMD for NRTI exposure (ever vs. never), along with the 95% credible intervals, are shown in red (scale = 0.280) and blue (scale = 0.587). (C) HR estimates derived from propensity score-matched models adjusted for the confounding variables listed in *SI Appendix, Supplementary Methods*, were estimated separately for each database. Inverse-variance-weighted random-effects and fixed-effect meta-analyses were performed to obtain a pooled estimate of the aHR of incident atrophic AMD for NRTI exposure (ever vs. never).



of heterogeneity). Second, the random-effects model is more appropriate as the databases represent populations with different underlying true effects (39–41). The random-effects meta-analysis revealed a protective effect of NRTIs (pooled aHR = 0.616; 95% CI, 0.493–0.770;  $P < 0.0001$ ) (Fig. 5A). For completeness, we also estimate a fixed-effect model, which also revealed a protective NRTI effect.

A Bayesian meta-analysis employing a random-effects normal-normal hierarchical model (42, 43) was performed. A half-Cauchy prior distribution for between-study variability assuming hazard ratios (HRs) between studies were unlikely to vary greater than threefold (scale = 0.280) was used. Collectively in the four databases, NRTI users had a reduced hazard of atrophic AMD [aHR, 0.615; 95% credible interval, 0.448, 0.850;  $P(\text{HR} > 1) = 0.007$ ] (Fig. 5B). A sensitivity analysis assuming HRs between studies were unlikely to vary greater than 10-fold (scale = 0.587) confirmed the directionality of the summary effect: NRTI use was protective [aHR, 0.615; 95% credible interval, 0.423, 0.902;  $P(\text{HR} > 1) = 0.013$ ] (Fig. 5B).

We used falsification outcomes to detect residual confounding (44–46). Appendicitis and hernia outcomes were selected as they are causally unrelated to NRTI exposure. Among HIV-negative patients not previously diagnosed with these outcomes, NRTI exposure was not associated with reduced risk of appendicitis or hernia (SI Appendix, Table S7).

Next, we used propensity-score matching, a causal inference approach used in observational studies (47–50), to create cohorts with similar baseline characteristics, reducing potential bias in estimating treatment effects (SI Appendix, Tables S8–S11 and Figs. S21–S24). To control further for residual covariate imbalance, we adjusted for all factors employed in the unmatched analyses. In all four databases, NRTI users had a reduced hazard of atrophic AMD (Fig. 5C and SI Appendix, Table S12). The combined risk, based on random-effects meta-analysis, revealed a protective effect of NRTIs (pooled aHR = 0.794; 95% CI, 0.664, 0.949;  $P = 0.01$ ), as did a fixed-effect model (Fig. 5C). The difference in the summary HR estimates between unmatched and propensity-score-matched analyses (0.616 vs. 0.794) suggests there could be residual bias in the unmatched analyses that was captured by propensity-score matching. However, the overlapping CIs of these summary HRs (0.493–0.770 vs. 0.664–0.949) suggests such residual bias is not significant.

## Discussion

The principal hazard of L1 to the human genome is perceived as mutagenic retrotransposition and enzymatic activity of the L1 ORF2-encoded endonuclease (EN) domain. Our findings suggest L1 RT activity itself may contribute to the pathological process of RPE degeneration independent of retrotransposition, thus potentially revealing a mechanism of human disease driven by reverse transcription of host genetic material. Previously, we demonstrated NRTIs could, by virtue of inhibiting inflammasome activation, block *Alu* RNA-induced RPE degeneration even when robbed of their RT-inhibitory activity (11). Our findings suggest NRTIs also protect against RPE degeneration by intercepting RT-dependent *Alu* cDNA synthesis upstream of inflammasome activation.

The evolutionarily recent *AluY* elements are the most retrotranspositionally active (18, 51). In contrast, the majority of Pol III-transcribed *Alu* RNAs is expressed from the more ancient *AluJ* and *AluS* elements (27–29). The similarity in the distribution of cytoplasmic *Alu* cDNA and *Alu* RNA subfamilies, i.e., the finding that the majority of both pools comprises elements of the more ancient J and S subfamilies, suggests that although the majority of Pol III-transcribed *Alu* elements lack sequence features important for retrotransposition capability (29) they remain reverse transcription competent. It also suggests that, in the cytoplasm, L1 RT has no preference for any *Alu* subfamily as a

substrate and that only the concentration of *Alu* transcripts from the respective *Alu* subfamily determines the fraction of *Alu* cDNAs resulting from reverse transcription of *Alu* RNAs. The fact that, contrarily, RNAs from young *AluY* elements that are underrepresented in the cytoplasmic pool of *Alu* RNAs and cDNAs are transmobilized by the L1 protein machinery more efficiently than the remaining *Alu* subfamilies suggests that there are either host-encoded nuclear factors necessary for the retrotransposition steps or cytoplasmic factors relevant for the transfer of the *Alu* ribonucleoprotein into the nucleus but not relevant for reverse transcription that have a bias for *AluY* sequences.

Our finding that *Alu* cDNA can be synthesized in the cytoplasm expands our understanding of the *Alu* replication cycle beyond the canonical model of TPRT-based *Alu* retrotransposition (35). More broadly, it will be interesting to address the possibility that various cytoplasmic RNAs (host or foreign) could be templates for cDNA formation. mRNAs can serve as substrates for L1-mediated retrotransposition, albeit at lower efficiency than *Alu* or L1 substrates (12, 52); future studies can determine the relative efficiency of cDNA formation from retroelements vs. other RNAs (53, 54). Although we demonstrate a pathogenic role for *Alu* cDNA, it might have functional roles in other settings. In high abundance, *Alu* cDNA could induce cell death to counteract excess L1 activity in cancers (55–57). Conversely, at low abundance, *Alu* cDNA might promote immunological self-tolerance to endogenous DNAs or prime immune factors for more rapid pathogen responses.

A strength of our health insurance database analyses is that findings were replicated in four independent cohorts diverse in age, gender, race, and time period, collectively representing a sizeable fraction of American adults with health insurance. The results of propensity score matching and falsification testing (which detects confounding, measurement error, selection bias) (44–46) increase the internal validity of this conclusion. Limitations include those inherent to health insurance database analyses, particularly accurate documentation, coding, and granularity of clinical phenotyping. Furthermore, despite confounder adjustment and robust propensity score matching, we cannot exclude the possibility of residual confounding or selection bias. Randomized controlled trials can yield better causal insights. Recently, we demonstrated NRTI use is associated with reduced development of type 2 diabetes (58). The current findings provide a rationale for prospective testing of NRTIs or alkylated NRTI derivatives, which block inflammasome activation but are less toxic than NRTIs (11), as potential therapies for geographic atrophy as well.

## Materials and Methods

Subretinal injections (1  $\mu\text{L}$ ) and/or intravitreal injections (0.5  $\mu\text{L}$ ) were performed in mice using a 35-gauge needle. Seven days after subretinal injection, RPE health was assessed by fundus photography and immunofluorescence staining of zonula occludens-1 (ZO-1) on RPE flat mounts. Quantification of RPE degeneration was performed as described previously (59).

For in situ hybridization the RPE from mice was collected at 24 h after subretinal injection. Cells in culture were collected after 6 to 8 h after *Alu* RNA transfection. Visualization of fluorescein-labeled probe was performed with the TSA plus fluorescence system under a confocal microscope.

The reaction to evaluate self-priming activity of *Alu* RNA was carried out in the absence of priming oligos in a 20- $\mu\text{L}$  reaction mix containing the following: *Alu* RNA with 3'-U tail; dNTP mix; cytoplasmic protein from mouse RPE cells; and Quantiscript RT Buffer (Qiagen). The resulting cDNA product was quantified by qPCR using *Alu* RNA template-specific primers.

This study used claims from the 1) Truven MarketScan Commercial Claims Database (IBM), which contains health care claims and medication usage obtained from analysis of commercial insurance claims from employer-based health insurance beneficiaries over the time period 2006 to 2018; 2) Veterans Health Administration system from 2000 to 2019, which contains data extracted from the Veterans Affairs Informatics and Computing Infrastructure (VINCI); 3) PearlDiver Patient Records Database, which captures health

care claims and medication usage for persons in the Humana network between 2007 and the first quarter of 2017; and 4) PearlDiver Mariner database, which captures health care claims and medication usage for persons in provider networks from 2010 to the second quarter of 2018. Study approval and waiver of Health Insurance Portability and Accountability Act authorization for the Veterans dataset were provided by the Dorn Veterans Affairs Medical Center Institutional Review Board. All data within the Truven and PearlDiver databases are Health Insurance Portability and Accountability Act-compliant and were thus deemed exempt from institutional review board's approval by the University of Virginia and University of South Carolina Institutional Review Boards. The completeness, utility, accuracy, validity, and access methods are described on these websites: <https://www.virec.research.va.gov/>; <https://www.ibm.com/products/marketscan-research-databases>; and <http://www.pearliverinc.com/researchinfo.html>.

The full materials and methods are provided in *SI Appendix*.

**Data Availability.** All data needed to evaluate the conclusions in this paper are available in the main text and *SI Appendix*.

**ACKNOWLEDGMENTS.** We thank J. L. Goodier and H. H. Kazazian for valuable discussions that improved the manuscript; A. P. Jackson, H. H. Kazazian, J. V. Moran, and M. A. Reijns for reagents and mice; and D. Robertson, K. Langberg, X. Zhou, R. Hankins, G. Pattison, Q. Zhong, K. A. Fox, and C. Spee for technical assistance. J.A. received support from NIH grants (DP1GM114862, R01EY022238, R01EY024068, R01EY028027, R01EY29799, and R01EY031039), the DuPont Guerry III Professorship, the University of Virginia Strategic Investment Fund, John Templeton Foundation Grant 60763, Doris Duke Distinguished Clinical Scientist Award, Ellison Medical Foundation Senior Scholar in Aging

Award, the DuPont Guerry III Professorship, Dr. E. Vernon Smith and Eloise C. Smith Macular Degeneration Endowed Chair, and a gift from Mr. and Mrs. Eli W. Tullis; S.F., from Japan Society for the Promotion of Science Fund for the Promotion of Joint International Research (Home-Returning Researcher Development Research) and Research Grant of Japan Eye Bank Association; N.K. received support from NIH Grants K99EY024336, R00EY024336, and R21EY030651, and the Beckman Initiative for Macular Research; B.J.F. received support from NIH Grants T32HL091812 and UL1RR033173; R.Y. received support from Association for Research in Vision and Ophthalmology/Alcon Early Career Clinician-Scientist Research Award; T.Y. received support from Fight for Sight postdoctoral award; R.K.S. received support from the Fulbright Visiting Scholar Program; D.R.H. received support from NIH Grant R01EY001545 and an unrestricted departmental grant from Research to Prevent Blindness; S.S.S. received support from resources and the use of facilities at the W. J. B. Dorn Veterans Affairs Medical Center, Dorn Research Institute; B.D.G. received support from NIH Grants R01EY028027 and R01EY031039, BrightFocus Foundation, the Owens Family Foundation, the American Heart Association, and the National Center for Research Resources and the National Center for Advancing Translational Sciences, NIH, through Grant UL1TR000117; and G.G.S. is supported by a grant from the Ministry of Health of the Federal Republic of Germany (FKZ2518FSB403). The content of this article is solely the responsibility of the authors and does not necessarily represent the official views of the NIH or the US Department of Veterans Affairs, nor does mention of trade names, commercial products, or organizations imply endorsement by the US government. This paper presents, in part, original research conducted using data from the Department of Veterans Affairs and is, in part, the result of work supported with resources and the use of facilities at the Dorn Research Institute, Columbia Veterans Affairs Health Care System (Columbia, SC). The funders had no role in study design, data collection and analysis, decision to publish, or preparation of the manuscript.

- H. H. Kazazian, Jr, J. V. Moran, Mobile DNA in health and disease. *N. Engl. J. Med.* **377**, 361–370 (2017).
- W. L. Wong *et al.*, Global prevalence of age-related macular degeneration and disease burden projection for 2020 and 2040: A systematic review and meta-analysis. *Lancet Glob. Health* **2**, e106–e116 (2014).
- J. Ambati, B. K. Ambati, S. H. Yoo, S. Ianchulev, A. P. Adamis, Age-related macular degeneration: Etiology, pathogenesis, and therapeutic strategies. *Surv. Ophthalmol.* **48**, 257–293 (2003).
- H. Kaneko *et al.*, DICER1 deficit induces Alu RNA toxicity in age-related macular degeneration. *Nature* **471**, 325–330 (2011).
- S. Dridi *et al.*, ERK1/2 activation is a therapeutic target in age-related macular degeneration. *Proc. Natl. Acad. Sci. U.S.A.* **109**, 13781–13786 (2012).
- V. Tarallo *et al.*, DICER1 loss and Alu RNA induce age-related macular degeneration via the NLRP3 inflammasome and MyD88. *Cell* **149**, 847–859 (2012).
- N. Kerur *et al.*, TLR-independent and P2X7-dependent signaling mediate Alu RNA-induced NLRP3 inflammasome activation in geographic atrophy. *Invest. Ophthalmol. Vis. Sci.* **54**, 7395–7401 (2013).
- J. D. Boeke, LINEs and Alus—the polyA connection. *Nat. Genet.* **16**, 6–7 (1997).
- P. Deininger, Alu elements: Know the SINEs. *Genome Biol.* **12**, 236 (2011).
- H. H. Kazazian, Jr, Mobile elements: Drivers of genome evolution. *Science* **303**, 1626–1632 (2004).
- B. J. Fowler *et al.*, Nucleoside reverse transcriptase inhibitors possess intrinsic anti-inflammatory activity. *Science* **346**, 1000–1003 (2014).
- M. Dewannieux, C. Esnault, T. Heidmann, LINE-mediated retrotransposition of marked Alu sequences. *Nat. Genet.* **35**, 41–48 (2003).
- C. R. Hagan, R. F. Sheffield, C. M. Rudin, Human Alu element retrotransposition induced by genotoxic stress. *Nat. Genet.* **35**, 219–220 (2003).
- M. E. Kleinman *et al.*, Sequence- and target-independent angiogenesis suppression by siRNA via TLR3. *Nature* **452**, 591–597 (2008).
- M. E. Kleinman *et al.*, Short-interfering RNAs induce retinal degeneration via TLR3 and IRF3. *Mol. Ther.* **20**, 101–108 (2012).
- W. An *et al.*, Characterization of a synthetic human LINE-1 retrotransposon ORFeus-Hs. *Mob. DNA* **2**, 2 (2011).
- A. Kirilyuk *et al.*, Functional endogenous LINE-1 retrotransposons are expressed and mobilized in rat chloroleukemia cells. *Nucleic Acids Res.* **36**, 648–665 (2008).
- E. A. Bennett *et al.*, Active Alu retrotransposons in the human genome. *Genome Res.* **18**, 1875–1883 (2008).
- T. Miyoshi, T. Makino, J. V. Moran, Poly(ADP-ribose) polymerase 2 recruits replication protein A to sites of LINE-1 integration to facilitate retrotransposition. *Mol. Cell* **75**, 1286–1298.e12 (2019).
- W. M. Liu, W. M. Chu, P. V. Choudary, C. W. Schmid, Cell stress and translational inhibitors transiently increase the abundance of mammalian SINE transcripts. *Nucleic Acids Res.* **23**, 1758–1765 (1995).
- J. J. Krolewski, C. W. Schindler, M. G. Rush, Structure of extrachromosomal circular DNAs containing both the Alu family of dispersed repetitive sequences and other regions of chromosomal DNA. *J. Mol. Biol.* **174**, 41–54 (1984).
- N. Kerur *et al.*, cGAS drives noncanonical-inflammasome activation in age-related macular degeneration. *Nat. Med.* **24**, 50–61 (2018).
- C. M. Rubin, C. M. Houck, P. L. Deininger, T. Friedmann, C. W. Schmid, Partial nucleotide sequence of the 300-nucleotide interspersed repeated human DNA sequences. *Nature* **284**, 372–374 (1980).
- M. A. Batzer *et al.*, Standardized nomenclature for Alu repeats. *J. Mol. Evol.* **42**, 3–6 (1996).
- M. A. Batzer, P. L. Deininger, Alu repeats and human genomic diversity. *Nat. Rev. Genet.* **3**, 370–379 (2002).
- X. O. Zhang, T. R. Gingeras, Z. Weng, Genome-wide analysis of polymerase III-transcribed Alu elements suggests cell-type-specific enhancer function. *Genome Res.* **29**, 1402–1414 (2019).
- A. Conti *et al.*, Identification of RNA polymerase III-transcribed Alu loci by computational screening of RNA-seq data. *Nucleic Acids Res.* **43**, 817–835 (2015).
- A. J. Oler *et al.*, Alu expression in human cell lines and their retrotranspositional potential. *Mob. DNA* **3**, 11 (2012).
- D. Mandal, A. Nasrolahi Shirazi, K. Parang, Cell-penetrating homochiral cyclic peptides as nuclear-targeting molecular transporters. *Angew. Chem. Int. Ed. Engl.* **50**, 9633–9637 (2011).
- A. Nasrolahi Shirazi *et al.*, Peptide amphiphile containing arginine and fatty acyl chains as molecular transporters. *Mol. Pharm.* **10**, 4717–4727 (2013).
- S. L. Martin, Ribonucleoprotein particles with LINE-1 RNA in mouse embryonic carcinoma cells. *Mol. Cell. Biol.* **11**, 4804–4807 (1991).
- J. Ambati, B. J. Fowler, K. Ambati, “Compositions and methods for treating retinal degradation” (University of Kentucky Research Foundation). US Patent 10,294,220 (2019).
- H. Schwartz *et al.*, Endogenous LINE-1 (long interspersed nuclear element-1) reverse transcriptase activity in platelets controls translational events through RNA-DNA hybrids. *Arterioscler. Thromb. Vasc. Biol.* **38**, 801–815 (2018).
- S. J. Boguslawski *et al.*, Characterization of monoclonal antibody to DNA-RNA and its application to immunodetection of hybrids. *J. Immunol. Methods* **89**, 123–130 (1986).
- Q. Feng, J. V. Moran, H. H. Kazazian, Jr, J. D. Boeke, Human L1 retrotransposon encodes a conserved endonuclease required for retrotransposition. *Cell* **87**, 905–916 (1996).
- V. Ahl, H. Keller, S. Schmidt, O. Weichenrieder, Retrotransposition and crystal structure of an Alu RNP in the ribosome-stalling conformation. *Mol. Cell* **60**, 715–727 (2015).
- M. R. Shen, J. Brosius, P. L. Deininger, BC1 RNA, the transcript from a master gene for ID element amplification, is able to prime its own reverse transcription. *Nucleic Acids Res.* **25**, 1641–1648 (1997).
- E. Vittinghoff, C. E. McCulloch, Relaxing the rule of ten events per variable in logistic and Cox regression. *Am. J. Epidemiol.* **165**, 710–718 (2007).
- C. Anello, J. L. Fleiss, Exploratory or analytic meta-analysis: Should we distinguish between them? *J. Clin. Epidemiol.* **48**, 109–116, discussion 117–118 (1995).
- R. DerSimonian, N. Laird, Meta-analysis in clinical trials. *Control. Clin. Trials* **7**, 177–188 (1986).
- J. Lau, J. P. Ioannidis, C. H. Schmid, Summing up evidence: One answer is not always enough. *Lancet* **351**, 123–127 (1998).
- A. J. Sutton, K. R. Abrams, Bayesian methods in meta-analysis and evidence synthesis. *Stat. Methods Med. Res.* **10**, 277–303 (2001).
- A. P. Dawid, The well-calibrated Bayesian. *J. Am. Stat. Assoc.* **77**, 605–610 (1982).
- V. Prasad, A. B. Jena, Prespecified falsification end points: Can they validate true observational associations? *JAMA* **309**, 241–242 (2013).
- M. Lipsitch, E. Tchetgen Tchetgen, T. Cohen, Negative controls: A tool for detecting confounding and bias in observational studies. *Epidemiology* **21**, 383–388 (2010).
- B. F. Arnold, A. Ercumen, J. Benjamin-Chung, J. M. Colford, Jr, Brief report: Negative controls to detect selection bias and measurement bias in epidemiologic studies. *Epidemiology* **27**, 637–641 (2016).

47. P. R. Rosenbaum, D. B. Rubin, The central role of the propensity score in observational studies for causal effects. *Biometrika* **70**, 41–55 (1983).
48. J. S. Haukoos, R. J. Lewis, The propensity score. *JAMA* **314**, 1637–1638 (2015).
49. H. Ohlsson, K. S. Kendler, Applying causal inference methods in psychiatric epidemiology: A review. *JAMA Psychiatry* **77**, 637–644 (2020).
50. K. Imai, D. A. van Dyk, Causal inference with general treatment regimes. *J. Am. Stat. Assoc.* **99**, 854–866 (2004).
51. M. K. Konkel *et al.*; 1000 Genomes Consortium, Sequence analysis and characterization of active human Alu subfamilies based on the 1000 Genomes pilot project. *Genome Biol. Evol.* **7**, 2608–2622 (2015).
52. W. Wei *et al.*, Human L1 retrotransposition: *cis* preference versus *trans* complementation. *Mol. Cell. Biol.* **21**, 1429–1439 (2001).
53. O. Dhellin, J. Maestre, T. Heidmann, Functional differences between the human LINE retrotransposon and retroviral reverse transcriptases for in vivo mRNA reverse transcription. *EMBO J.* **16**, 6590–6602 (1997).
54. C. Esnault, J. Maestre, T. Heidmann, Human LINE retrotransposons generate processed pseudogenes. *Nat. Genet.* **24**, 363–367 (2000).
55. P. E. Carreira, S. R. Richardson, G. J. Faulkner, L1 retrotransposons, cancer stem cells and oncogenesis. *FEBS J.* **281**, 63–73 (2014).
56. F. Di Ruocco *et al.*, Alu RNA accumulation induces epithelial-to-mesenchymal transition by modulating miR-566 and is associated with cancer progression. *Oncogene* **37**, 627–637 (2018).
57. B. Rodriguez-Martin *et al.*; PCAWG Structural Variation Working Group; PCAWG Consortium, Pan-cancer analysis of whole genomes identifies driver rearrangements promoted by LINE-1 retrotransposition. *Nat. Genet.* **52**, 306–319 (2020).
58. J. Ambati *et al.*, Repurposing anti-inflammasome NRTIs for improving insulin sensitivity and reducing type 2 diabetes development. *Nat. Commun.* **11**, 4737 (2020).
59. S. Narendran *et al.*, A clinical metabolite of azidothymidine inhibits experimental choroidal neovascularization and retinal pigmented epithelium degeneration. *Invest. Ophthalmol. Vis. Sci.* **61**, 4 (2020).